The bacterial molecular switch DnaA-ATP integrates chromosome replication with cell growth and division dynamics

Ezza Khan and Paola E. Mera*

Department of Microbiology, University of Illinois at Urbana-Champaign, Urbana, IL, USA
* Corresponding author e-mail address: pmera@illinois.edu

KEY WORDS. Cell size, constriction rate, DnaA, transcription factor, molecular switch, peptidoglycan, MurD, *C. crescentus,* FtsZ

ABSTRACT

Successful proliferation of bacteria requires the coordination of multiple cellular events. The precise coordination between the replication of the chromosome with cell growth and division is essential for daughter cells to inherit an intact copy of the genome with the appropriate cell size. However, the molecular mechanisms that temporally and spatially integrate these essential processes have remained elusive in the field. Using the model system *C. crescentus*, we uncovered a previously unrecognized role for the conserved chromosome replication initiator DnaA in regulating cell growth and division dynamics. Through mutant analyses, transcriptional profiling, biochemical and high-resolution imaging, our data demonstrate that DnaA modulates cell size through direct transcriptional activation of enzymes involved in cell wall biosynthesis. We identify a conserved cell wall biosynthetic enzyme, MurD, as a key downstream effector and demonstrate its unexpected ability to restrict cell size. Both *in vivo* and *in vitro* analyses revealed that the transcriptional regulation of *murD* requires the ATP-bound form of DnaA, the same nucleotide-bound form required for initiating chromosome replication. These findings highlight how bacteria leverage the conserved nucleotide-dependent switch, DnaA-ATP, to temporally orchestrate spatially distinct processes ensuring accurate progression of the cell cycle.

INTRODUCTION

Bacteria must tightly coordinate multiple cellular processes to ensure successful progression of the cell cycle. This coordination involves the regulation, temporally and spatially, of key events like chromosome replication and segregation, as well as the elongation and constriction of the cell envelope[1]. A critical component of this regulatory circuitry includes the biosynthesis and maintenance of precursors that are necessary to sustain the forward progression of the cell cycle. In addition to the intracellular multi-level coordination, bacteria actively integrate environmental cues into the cell cycle regulatory circuitry to quickly adapt to changing conditions [2]. How bacteria manage to coordinate all these processes while growing and dividing at such rapid rates remains a fascinating challenge for scientists to unravel. In this study, we aimed at uncovering molecular details of such strategies.

One of the first committed steps in the bacterial cell cycle is the initiation of chromosome replication, a process regulated by the conserved initiator protein DnaA [3-5]. DnaA bound to ATP (DnaA-ATP) oligomerizes at the origin of replication (*oriC*), opens *oriC,* and allows the replication machinery to assemble and initiate chromosome replication [3,4]. Following initiation of replication, the protein Hda bound to the β-clamp of the replisome turns off DnaA by promoting DnaA's intrinsic ATPase activity [6,7]. Besides its role in chromosome replication, DnaA serves as a conserved transcription factor [8,9], albeit fewer mechanistic details are known about this function. The DnaA transcriptional regulon commonly comprises genes encoding components of the replisome and enzymes involved in nucleotide biosynthesis [9,10,11] . Interestingly, both functions of DnaA (replication initiation and transcriptional regulation) are modulated by DnaA's nucleotide-bound state: ATP binding and hydrolysis are essential for its activity as a replication initiator[12,13], while the identity of the bound nucleotide (ATP vs. ADP) can influence its function as a transcription factor[14-16].

The ability of bacteria to double in size and undergo division relies on the coordinated assembly and remodeling of their cell wall [17]. The cell wall is primarily composed of peptidoglycan (PG), a polymer of glycan strands consisting of alternating N-acetylglucosamine and N-acetylmuramic acid (GlcNAc & MurNAc) residues, cross-linked by short peptides [18]. PG biosynthesis begins in the cytoplasm with the production of the nucleotide-linked precursors UDP-GlcNAc and UDP-MurNAc, which are subsequently assembled into lipid II by membrane-associated enzymes, and ends in the periplasm where protein complexes coordinate cell wall remodeling during growth and division [19,20,21]. In rod-shaped bacteria, new cell wall material is typically inserted laterally during cell elongation by the Rod complex, which includes the actin homolog MreB [22,23]. Subsequently, PG synthesis shifts to the midcell driven by the divisome machinery, which includes the tubulin homolog FtsZ [24]. The molecular mechanisms that temporally integrate chromosome replication initiation with cellular expansion and division remain poorly understood.

Identifying the molecular mechanisms that coordinate multiple events over the progression of the cell cycle is inherently challenging due to the intricate and overlapping nature of these processes.

However, the diderm oligotrophic bacterium *Caulobacter crescentus* offers a powerful model system that enables high-resolution analysis of cell cycle regulation due to its well-defined developmental stages and robust genetic tools[25-29]. Upon cell division, *C. crescentus* produces two genetically identical but morphologically distinct cells: a smaller motile swarmer cell that cannot initiate chromosome replication and a sessile stalk cell that is replication competent[29] (Figure 1A). The dimorphic life cycle of *C. crescentus* enables isolation of homogeneous populations of cells at different developmental stages [30-33]. Furthermore, *C. crescentus* initiates chromosome replication once per cell cycle regardless of nutrient conditions [34] enabling detailed investigation into the mechanisms that coordinate onset of chromosome replication with cellular growth and the progression of the cell cycle.

A recurring theme in biology is that nature often achieves remarkable complexity through elegantly simple regulatory mechanisms. In this study, we uncovered one such mechanism in which the conserved initiator of chromosome replication DnaA regulates growth and constriction rate through the transcriptional regulation of cell wall biosynthetic enzymes. Specifically, we identify MurD, a key enzyme in the conserved cytoplasmic pathway for peptidoglycan precursor biosynthesis, as a direct target of DnaA. Our findings reveal that MurD plays an unexpected role in the regulation of cell size. Collectively, this work demonstrates a direct regulatory axis linking chromosomal maintenance to cell growth and size, positioning the molecular switch DnaA-ATP as a central integrator of the bacterial cell cycle.

RESULTS

DnaA impacts cell size without changing oriC copy number

A common strategy to study the essential protein DnaA is to use constructs where the native *dnaA* gene is knockout and a *dnaA* copy is engineered to be expressed from inducible promoters. While characterizing such constructs, we noticed that cells expressing *dnaA* from the inducible promoter vanillate are smaller compared to wildtype cells with *dnaA* at its native locus (Figure 1B). The quantification of cell size revealed that cell length decreased ~20 % (Figure 1C) whereas the width remained the same (Figure S1A). To ensure that this effect was not in response to the inducer vanillate, we analyzed cells expressing *dnaA* from the other commonly used promoter, P_{xylose} [35]. Our data revealed that cells expressing *dnaA* from either inducible promoter displayed the same reduction in cell length (Figure S1B,C).

Given that DnaA initiates replication at *oriC* and *oriC* copy number are correlated with cell size [36], we examined the possibility that changes in *oriC* copy number caused the change in cell size. In *C. crescentus*, replication initiates only once per cell cycle resulting in cells with one or a maximum of two *oriC* copies [34]. To quantify *oriC* copy number, we used the centromere-like region *parS* (~8 kilobases away from *oriC*) as proxy of number of origins of replication [37,38]. We fluorescently labeled the *parS*-binding protein ParB and tracked the number of CFP-ParB foci. Our data showed that cells expressing *dnaA* from inducible promoters display wildtype numbers of *oriC* copies per cell (Figure 1D), discarding the possibility that changes in *oriC* copy number are responsible for the effect on cell length.

111 Taking advantage of *C. crescentus* asymmetric cell cycle, we examined whether the DnaA-
112 dependent impact on cell length was specific to the developmental stage of the cell. We wondered
113 about this possibility based on the recent findings that *C. crescentus* shows differential growth
114 rates through their cell cycle [39,40]. To test this hypothesis, we analyzed cell size of isolated
115 homogeneous population of swarmer cells [30,31]. Our analysis revealed that swarmer cells display
116 a similar ~20% reduction in cell length (Figure 1E) demonstrating that the impact on cell size is
117 not specific to the developmental stage of the cell. Collectively, these data revealed that changing
118 *dnaA's* transcriptional regulation result in a reduction of cell length independent of both *oriC* copy
119 number and cell cycle stage.

120

121 *Cell length inversely correlates with DnaA abundance*

122 The levels and activity of DnaA as the replication initiator are regulated at a multitude of levels,
123 including post-transcriptionally and post-translationally [41,42]. Given that our observed reduction in
124 cell length was potentially linked to *dnaA*'s transcriptional regulation (native vs. inducible
125 promoter), we examined whether the levels of the protein DnaA had changed when expressed
126 from inducible promoters. Using western blot analysis with antibodies specific to DnaA, we found
127 that the small cells display ~3-fold higher levels of DnaA compared to wildtype grown under the
128 same condition (Figure S1D,E), suggesting increased DnaA levels were causing changes in cell
129 length. We next examined whether the changes in cell length are proportional with the cellular
130 levels of DnaA under conditions that do not impact *oriC* copy number. We titrated the induction
131 levels of *dnaA* expression and confirmed the corresponding increase in DnaA protein levels using
132 western blot analysis (Figure 1F). Notably, as the levels of DnaA increase, we observed a
133 corresponding decrease in cell length (Figure 1G). We were able to reach the highest expression
134 levels of DnaA (without over-initiation of chromosome replication) when cells were grown with the
135 inducer xylose as the sole carbon source (no glucose added to avoid repression of the xylose
136 promoter [43]). Our analysis showed that the highest DnaA concentration also results in the highest
137 decrease in cell length (Figure 1H). Collectively, these data demonstrate that the observed
138 changes in cell length are dependent on the cellular levels of the protein DnaA. From here on, we
139 will refer to cells expressing *dnaA* from inducible promoters (*xyl* or *van*) that exhibit a 3-fold
140 increase in DnaA levels as 3x-DnaA cells.

141

142 *Cell size control pathways and their relevance to 3x-DnaA cells.*

143 Building on our observation that increased DnaA levels reduce cell length, we next examined
144 whether this DnaA-dependent effect intersects with known bacterial cell size control pathways.
145 For instance, reducing the total protein content in the cell has been shown to correlate with a
146 reduction in cell size [44]. In *B. subtilis,* reducing the synthesis of proteins (using subinhibitory levels
147 of the ribosome targeting antibiotic chloramphenicol) results in ~10% cell length reduction without
148 changes in cell width [45]. Analogous to *B. subtilis*, our analysis of wildtype *C. crescentus* cells
149 exposed to sub-lethal concentrations of chloramphenicol revealed a reduction in cell length by
150 approximately 10%, while cell width remained unchanged (Figure S2A). Notably, chloramphenicol

151 treatment further exacerbated the size reduction in 3x-DnaA cells compared do untreated
152 conditions (Figure S2B). These results revealed that DnaA's effect on cell size is independent
153 from the effect that protein content has on cell size regulation. To assess the impact of additional
154 cell size determinants on the reduced length of 3x-DnaA cells, we performed supplementary
155 analyses using genetic approaches, growth media types, and small molecule inhibitors (see
156 Supplemental Information for experimental details). The results of these experiments ruled out
157 contributions from the stringent response (Figure S2C) and nutrient availability (Figure S3), but
158 left open the possibility of envelope biosynthesis (Figure S4), which is addressed in detail later in
159 this manuscript.

160

161 *The ability of DnaA to bind both ATP and DNA are required for its impact on cell size*

162 To gain insights into the mechanism of how DnaA influences cell size, we examined the functional
163 contributions of its distinct domains (Figure 2A) by constructing a set of variants featuring domain-
164 specific truncations or targeted amino acid substitutions. Because DnaA is essential and minor
165 modification to any of these domains can impact viability, we analyzed the effects on cell size
166 using chromosomal *dnaA* merodiploid strains. These merodiploid strains express variants of
167 DnaA from an inducible chromosomal promoter (P_{xyl}) while the native copy of *dnaA* remains intact.
168 Our data revealed that this type of constructs with wildtype *dnaA* expressed from *Pxyl* (*parB::cfp-*
169 *parB* P_{xyl}*-dnaA*) also display the ~20% reduction in cell length when DnaA levels are increased
170 ~3-fold (Figure S5A, B). We confirmed that the expression of DnaA variants from P_{xyl} have no
171 dominant negative effect on viability using colony forming units (CFU) (Figure 2B). Expression
172 and accumulation of DnaA protein variants compared to empty vector control (EV) were confirmed
173 with western blots (Figure 2C).

174 In *C. crescentus*, an alanine-rich region at the N-terminal end of domain I has been shown to
175 regulate the cellular levels of DnaA upon nutrient starvation [46]. We reasoned that if this ala-rich
176 domain was involved in triggering the change in cell size, increasing the levels of a truncated
177 version of DnaA missing this alanine rich region would have no effect on cell length. However,
178 cells expressing a truncation of the alanine rich region expressed from P_{xyl} (referred as ∆ala)
179 retained their ability to reduce their cell length (Figure 2D), albeit to marginally lower levels. The
180 small difference in cell length reduction (~18% vs. ~22%) can be attributed to lower levels of
181 expression of this variant compared to cells with 3x-wildtype-DnaA (Figure 2C). These data further
182 support that the impact on cell length is dependent on DnaA levels, and that the alanine rich N-
183 terminal domain is not responsible in DnaA's regulation of cell length.

184 We considered another possibility where DnaA's role with cell size regulation was independent of
185 its ability to bind DNA. We posit that DnaA itself could regulate cell size potentially by directly
186 modulating the activity of cell size regulators independent of DNA binding. We tested this
187 hypothesis by analyzing the effect on cell length from a DnaA with the DNA-binding domain
188 (domain IV) truncated (referred as ∆IV). Expression of this truncated variant unable to bind DNA
189 had no effect on cell length compared to wildtype levels of DnaA (Figure 2D), revealing that
190 DnaA's ability to bind DNA is required for its role with cell size regulation. Wondering whether ATP
191 binding and/or hydrolysis was required for DnaA's impact on cell length, we analyzed a variant

192 with a single amino acid substitution that interrupts ATP binding. We did not analyze DnaA
193 variants unable to hydrolyze ATP because such variants are stuck in the active form and over-
194 initiate chromosome replication, which would inevitably impact cell size in an *oriC* copy dependent
195 manner. We constructed DnaA-K195I, a variant encoding a mutation in the Walker A box that
196 affects DnaA's ability to bind ATP [47]. Our data revealed that DnaA-K195I lost the effect on cell
197 length and cells expressing this variant displayed wildtype cell size (Figure 2D).

198 Collectively, the analyses of DnaA variants revealed that DnaA requires to bind DNA and to bind
199 ATP to cause the effect on cell size. Given that DNA-binding and ATP-binding are involved in
200 regulating both functions of DnaA (chromosome replication initiator and transcription factor), we
201 set out to differentiate DnaA's effect on cell length between these two functions. Because we
202 cannot uncouple these two functions without altering the proper progression of the cell cycle and
203 thus cell growth regulation, we proceeded by analyzing each function independently.

204

205 *Chromosome replication remains unchanged in 3x-DnaA cells*

206 The initiation of chromosome replication requires DnaA-ATP oligomerization at *oriC*, which opens
207 the double stranded DNA allowing for components of the replisome to assemble and to initiate
208 replication bidirectionally [48]. We explored the possibility that 3x-DnaA levels could alter the overall
209 process of chromosome replication, potentially leading to the reduction in cell size. To test this
210 hypothesis, we used time-lapse microscopy to image synchronized swarmer cells throughout their
211 cell cycle, focusing on three key events of chromosome replication: (a) timing of replisome
212 assembly, (b) timing of replication initiation, and (c) progression of the replication forks (Figure 3).
213 To track replisome assembly, we imaged a strain encoding the replisome component DnaN (β-
214 clamp) fluorescently tagged at *dnaN's* native chromosomal locus [49,50]. Our analysis of the time
215 when the DnaN-mCherry focus emerges revealed that the 3x-DnaA small cells and wildtype cells
216 assembled their replisomes at similar times (Figure 3A). To determine timing of replication
217 initiation, we tracked the appearance of two *parS* loci (8kb from *oriC*) using the *parS*-binding
218 protein CFP-ParB [37]. Our data revealed the 3x-DnaA small cells initiate chromosome replication
219 at similar times as wildtype cells (Figure 3B). Lastly, we examined replisome progression by
220 comparing when a chromosomal locus near the gene *pleC* (1.3 Mb from *oriC*) is replicated. To
221 track replication of *pleC*, we used a strain engineered to encode the Yersinia pestis sequence of
222 *parS(*pMT1) near the *pleC* locus and the corresponding ParB(pMT1) fluorescently labelled
223 expressed from an inducible promoter [51]. We included to this strain a fluorescent tag with the *C.*
224 *crescentus'* native ParB as an internal control. Analyzing the timing of replication of *parS* and *pleC*
225 revealed no difference between wildtype and 3x-DnaA small cells (Figure 3C). Overall, these data
226 indicate that the higher levels of DnaA in 3x-DnaA small cells do not alter the overall process of
227 chromosome replication.

228

229

230 *3x-DnaA cells display changes in transcriptional profiles*

231 After demonstrating that 3x-DnaA levels do not affect the progression of chromosome replication,
232 we proceeded to investigate DnaA's other conserved role as a master transcriptional regulator.
233 [52-54]. DnaA transcriptional regulon typically includes genes encoding components of the
234 replisome, cell cycle regulators, and nucleotide biosynthesis [54 55 56]. To test the hypothesis that
235 DnaA regulates cell size through its activity as a transcription factor, we examined transcriptional
236 changes in 3x-DnaA small cells. For these analyses, we used the *dnaA* merodiploid strains to
237 enable cell growth and comparisons with the DnaA variants. When comparing 3x-DnaA (P_{xyl}-
238 $dnaA^{WT}$) with an empty-vector control, our RNA-Seq analysis revealed relatively few genes
239 change expression: 45 total genes with 35 upregulated and 10 downregulated (≥1.5-fold change
240 and FDR<0.05). To further exclude non-contributing factors responsible for changes in cell length,
241 we compared RNA-Seq changes between P_{xyl}-$dnaA^{WT}$ cells (exhibit reduced size) and P_{xyl}-*dnaA*-
242 *K195I* (exhibit unaffected cell size due to variant's inability to bind ATP). Using this strategy with
243 the same parameters of ≥1.5-fold change and FDR<0.05, our list of potential genes was reduced
244 to 23 (Figure 4A, Table S1). From this list we focused on genes involved in cell cycle progression.
245 To validate our hits, we used constructs with chromosomal merodiploid strains to circumvent the
246 high expression levels associated with replicating plasmids, given that the genes of interest
247 exhibited changes of approximately 2-fold.

248 The 1.5-fold increase in *ftsZ* expression in 3x-DnaA cells immediately stood out for multiple
249 reasons. First, *ftsZ* is part of the transcriptional regulon of DnaA [54]. Second, the transcriptional
250 regulation of *ftsZ* is dependent on the nucleotide-bound to DnaA [14]. Third, FtsZ is a key regulator
251 of the divisome, the molecular machinery that drives cytokinesis and cell wall biosynthesis at the
252 septum [57], both functions that can directly impact cell size [58,59]. To characterize the potential role
253 of FtsZ, we first examined whether the levels of the FtsZ protein were higher in 3x-DnaA cells
254 compared to empty vector, like our transcriptomics data suggested. However, western blot
255 analysis using FtsZ-specific antibodies revealed no detectible difference in FtsZ protein levels
256 between 3x-DnaA cells and the control (Figure 4B). To further characterize whether elevated
257 levels of FtsZ could lead to a reduction in cell size, we constructed a chromosomal *ftsZ*
258 merodiploid strain that displayed subtle increases in FtsZ levels (Figure S6A). Our data revealed
259 that increasing FtsZ levels does not decrease cell length (Figure 4C). Instead, cells with increased
260 FtsZ levels retain similar size as wildtype but they generate mini-cells (Figure S6B), consistent
261 with previous reports [60]. These data demonstrate that the DnaA-dependent changes in cell size
262 occur independently of changes in levels of FtsZ.

263

264 *MurD is a key regulator that impacts cell size in a DnaA-ATP-dependent manner*

265 The transcriptional analysis of 3x-DnaA cells revealed changes in two peptidoglycan (PG)
266 biosynthetic genes located adjacent to each other: *murD* (+1.5-fold) and *mraY* (+1.6-fold). MurD
267 is one of the four cytoplasmic ATP-dependent enzymes that catalyze the successive additions of
268 amino acids to UDP-N-acetylmuramic acid in PG biosynthesis [61]. MraY transfers UDP-N-
269 acetylmuramic acid-pentapeptide onto the lipid carrier bactoprenol forming the intermediate
270 known as lipid I [62]. To test the hypothesis that changes in MurD or MraY levels were responsible

271 for the changes in cell size observed in 3x-DnaA small cells, we constructed chromosomal
272 merodiploid strains of each to titrate the levels of these proteins using wildtype expression of *dnaA*
273 as the parent strain. Induction of *mraY* expression in the *mraY* merodiploid strain did not reduce
274 cell length but instead caused a subtle but significant increase in cell length compared to empty
275 vector (Figure 4C). Remarkably, analysis of the *murD* merodiploid strain revealed that induced
276 increased expression of *murD* alone results in cells with ~10% reduction in cell length. We show
277 that MurD's ability to restrict cell length is independent of nutrient availability (Figure S7).

278 Altering the expression of *murD* was the only genetic modification from our RNA-Seq analysis
279 that led to a decrease in cell size (see other genes tested in Supplemental information and Figures
280 S6) Wondering whether we could achieve an even greater reduction in cell size by further
281 increasing *murD* expression beyond the already higher levels in 3x-DnaA cells, we constructed a
282 *murD* merodiploid strain using the 3x-DnaA cells as the parent strain (*dnaA* expressed from
283 inducible promoter). Our data revealed that indeed, induction of *murD* overexpression in the 3x-
284 DnaA cells results in an additional ~10% decrease in cell length generating even smaller cells
285 than 3x-DnaA cells (Figure 4D). However, the higher induction of *murD* in 3x-DnaA cells and/or
286 their smaller cell size led to a defect in doubling rate (Figure 4E), demonstrating the importance
287 of maintaining proper levels of MurD and cell size for optimal growth.

288

289 *DnaA-ATP regulates the transcription of murD*

290 Having identified MurD as a key factor in regulating size in 3x-DnaA cells, we next examined the
291 relationship between *murD* expression and DnaA. We initially hypothesized that DnaA regulates
292 *murD* expression indirectly through the transcription factor GcrA [25]. This hypothesis was based
293 on two observations: first, gcrA transcript levels were elevated 1.8-fold in 3x-DnaA cells (Figure
294 4A); second, *murD* is part of the division and cell wall (dcw) cluster [18], and in *C. crescentus,* its
295 expression has been predicted to be under GcrA control [63]. To test our hypothesis, we modulated
296 GcrA levels independently of DnaA and quantified *murD* transcripts using RT-qPCR. These
297 analyses revealed that changes in GcrA abundance had no detectable effect on *murD* expression
298 (Figure 5A). In contrast, altering DnaA levels result in clear changes in *murD* transcript levels
299 (Figure 5B), suggesting a direct regulatory role for DnaA.

300 Given that *murD* is part of an operon (Figure 5C), we were intrigued that
301 only *mraY* and *murD* were significantly upregulated in 3x-DnaA cells (Figure 4A). This selective
302 expression suggested that these genes are transcribed independently of the rest of the operon.
303 Supporting this hypothesis, previously reported +1 transcriptional start sites (TSS) were identified
304 upstream of the *mraY* gene[64]. Furthermore, we identified a DnaA binding motif upstream of the
305 translational start codon of *mraY* (Figure 5C), with structural organization previously shown with
306 other genes regulated by DnaA [54]. To directly test the model that DnaA can bind upstream of
307 *mraY-murD*, we cloned the region upstream of *mraY* into a plasmid and tested direct binding using
308 electrophoretic mobility shift assays (EMSA) with purified DnaA[65] .

309 Our EMSA analysis confirmed that DnaA binds upstream of *mraY-murD*, supporting DnaA's role
310 as a transcriptional regulator (Figure 5D). Furthermore, we discovered that DnaA's ability to bind

upstream of *mraY-murD* is significantly increased when DnaA is bound to ATP (Figure 5D), indicating that nucleotide binding is essential for DnaA's regulatory activity of *mraY-murD* expression. This ATP requirement is remarkably consistent with our analyses of cells expressing the ATP-binding deficient variant DnaA-K195I that was unable to influence cell size (Figure 2D) and displayed no differences in *mraY* and *murD* transcriptional levels compared to wildtype or to 3x-DnaA cells (Table S1). These findings reinforce the essential role of ATP in enabling DnaA to function as a transcriptional regulator of cell wall biosynthesis.

3x-DnaA small cells constrict at a faster rate during cell division than WT.

Constriction rate plays a critical role in the regulation of cell size in bacteria [28]. Given that our 3x-DnaA cells display smaller size, we investigated whether the reduction in size could be attributed to a change in constriction dynamics. To determine rate of constriction, we imaged synchronized 3x-DnaA cells and wildtype cells through a complete cell cycle starting from the G1 phase (swarmer state) through the completion of cytokinesis. Each individual cell was then analyzed through the progression of its cell cycle using the Fiji plugin MicrobeJ [66,67]. Using automated 5-min interval time-lapse image data, our analysis revealed that 3x-DnaA cells constrict at a significantly faster rate (10.1 $\pm$ 0.6 nm/min) than wildtype cells (7.4 $\pm$ 0.5 nm/min), representing an increase of approximately 26% (Figure 6C). In *C. crescentus,* faster constriction rates are correlated with slower elongation rates [68-70]. Our analysis of elongation rate demonstrated that, 3x-DnaA cells elongate at a slower rate (8.1 $\pm$ 0.7 nm/min) compared to wildtype cells (10.7 $\pm$ 1.0 nm/min) (Figure 6D). Collectively, these findings support that DnaA's transcriptional regulation of PG biosynthetic enzymes can modulate cell size by altering the cell growth and division dynamics.

DISCUSSION

In this study, we investigated how elevated levels of DnaA, without disrupting chromosome replication, result in a consistent ~20% reduction in cell size. Using the genetically tractable model *C. crescentus*, we dissected the overlapping events of the bacterial cell cycle and found that ATP-bound DnaA not only initiates chromosome replication but also influences cell growth and constriction rate by regulating the transcription of genes involved in cell wall biosynthesis. Notably, we identified MurD, a conserved enzyme in cell wall biosynthesis, as a previously unrecognized determinant that restricts cell size. Our data support the model that DnaA functions as a transcriptional regulator of *murD*, and that this regulatory activity is dependent on its ATP-bound state.

We propose that DnaA orchestrates a broad transcriptional program, integrating modest shifts across multiple targets to coordinate cell growth. While increased *murD* expression alone led to ~10% reduction in cell size, increased DnaA levels produced a more pronounced ~20% decrease. Our transcriptional analyses revealed subtle (<2-fold) changes in genes involved in cell wall biosynthesis and cell cycle progression in cells with increased DnaA levels (Table S1). Although none of these genes individually recapitulated the full phenotype and most caused cell filamentation when perturbed (Figure S6), their collective regulation likely contributes to the

349 observed size reduction. This is consistent with the complexity of cell growth, which requires the
350 synchronized activity of diverse enzymes and protein complexes.

351 Bacteria have been known to follow the Growth law, which states that cell size is an exponential
352 function of growth rate [71-75]. In this study, we show that MurD's impact on cell size is independent
353 of nutrient availability (Figure S7). Cells with increased *murD* expression in wildtype background
354 reduced their size when grown in minimal or rich media. We discovered that further increase of
355 *murD* expression results in a further reduction in cell size that was interestingly accompanied by
356 a decrease in growth rate. This phenomenon may be attributed to the reduced cellular volume
357 interfering with essential housekeeping processes during the cell cycle or a potential connection
358 between MurD and the Growth Law. MurD has gathered significant attention in drug development
359 due to its crucial role in cell wall biosynthesis [76,77]. Further investigation into MurD's activity and
360 its role in cell size regulation will yield significant insights into the complex mechanisms that govern
361 the progression of the bacterial cell cycle.

362 The link between rates of growth/constriction and enzymes involved in the biosynthesis of PG
363 precursors has been observed across different bacterial species[78]. In *B. subtilis*, the growth rate
364 is dependent on the abundance of lipid II and of the levels of the first committed PG biosynthetic
365 enzyme, MurA [79]. In *P. aeruginosa*, MraY, the enzyme that synthesizes Lipid I, maintains a
366 balance in cell wall homeostasis and growth [80]. In *Staphylococcus aureus*, MurJ , the membrane-
367 bound protein that flips Lipid II from the cytoplasm to the periplasm, has been linked to
368 accelerating constriction rate independent of FtsZ-treadmilling [81 82]. In *C. crescentus*, a positive
369 correlation was shown between constriction rate and PG proteins FtsWI [68] and their regulator FzlA
370 [70 83]. The work presented here demonstrates that the PG biosynthetic enzyme MurD is also linked
371 to the regulation of growth/constriction rates. Furthermore, our data uncovered an additional layer
372 of regulation that integrates chromosome replication into the coordination between PG
373 biosynthesis and growth/division, underscoring the sophisticated mechanisms bacteria employ to
374 sustain rapid and accurate proliferation.

375 The discovery that DnaA modulates cell growth and division adds to its growing reputation as a
376 global regulator of bacterial cell development, extending beyond its role with chromosome
377 replication. For instance, DnaA's transcriptional regulon commonly includes other global
378 regulators involved in genome maintenance, cell development, and pathogenesis [54,84,85] . In *B.*
379 *subtilis*, DnaA is connected to the onset of sporulation by transcriptionally regulating an inhibitor
380 of the sporulation master transcription factor SpoOA[53]. In *Borrelia burgdorferi*, DnaA regulates the
381 transcription of the nucleoid associated protein EbfC which itself regulates the transcription of a
382 multitude of other genes [84,86]. Furthermore, altering the transcriptional activity of DnaA in *B.*
383 *burgdorferi* led to changes in >20 components of the elongasome and divisome, which could also
384 connect DnaA to cell wall biosynthesis [87]. Beyond bacteria, replication initiators in eukaryotes
385 (Origin Recognition Complex, ORC) also perform roles beyond DNA replication, influencing
386 multiple cellular events including chromosome repair, condensation, segregation, and
387 cytokinesis[88-92]. These functional parallels across domains of life emphasize the role that
388 chromosome replication initiators play as central integrators of the cell cycle.

RESOURCE AVAILABILITY

All data are contained within the manuscript.

ACKNOWLEDGEMENTS

We are grateful to Prof. Erin Goley and her lab for providing the FtsZ antibodies, specifically to Dr. Jordan M. Barrows for his assistance with the rate of elongation and constriction protocol. We thank Anuradha Sharma from the Prof. Sanfilippo lab for her help with the RT-qPCR, Dr. Alvaro Hernandez from the Roy J. Carver Biotechnology Center for RNA sequencing, as well as to Dr. Jenny Drnevich for her expertise in the statistical analysis of the RNA-seq data. We thank Sasha Agafonova for her contribution in the construction of the graphical abstract. The work reported in this publication was supported by the National Institute of General Medical Sciences of the National Institutes of Health (NIH) under Award Numbers R01 GM133833 & R3GM158016, and by the National Science Foundation (NSF) Science and Technology Center for Quantitative Cell Biology under Award Number 2243257.

AUTHOR CONTRIBUTIONS

EK and PEM conceived project and wrote manuscript. EK performed all experiments and data analyses.

DECLARATION OF INTERESTS

The authors declare no completing interests.

FIGURE LEGENDS

Figure 1. DnaA impacts cell size without changing *oriC* copy number. A. (Left) Schematic representation of *Caulobacter* dimorphic lifestyle. **B**. Phase contrast images of WT (*parB*::CFP-*parB*) and *dnaA* inducible strain (*dnaA*::Ω, *parB::cfp-parB,* P_{van} *dnaA)* grown in minimal media (M2G) to exponential phase, scale 2µm. **C.** Super plots showing cell length analysis of mixed population. Small dots represent data points from three independent replicates, large dots represent median values (blue, pink, yellow). The horizontal line represents the mean of three median values. *dnaA* inducible shows ~20% decrease in cell length. **D.** Percentage cells representing *oriC* quantification in WT and inducible *dnaA* strain showing non-significant change. **E**. Super plots showing cell length analysis of synchronized population grown in M2G. *dnaA* inducible swarmer's show 20% decrease in cell length. **F.** Western Blot showing DnaA titration using WT and inducible *dnaA* (*dnaA*::Ω, *parB::cfp-parB,* P_{xyl} *dnaA*). Cells were grown in M2G with xylose titrated from 0.025%, 0.05%, 0.075% to 0.3% in M2G, to exponential phase. For maximum expression cells were grown in M2X to shown after dotted line. **G.** Super plots showing cell length analysis of DnaA titration. Small dots represent data points from three independent replicates, large dots represent median values (blue,grey,orange). At 0.025% xylose cell length is comparable to WT, M2X shows decrease in cell length ~20%. **H.** Quantification of DnaA levels left panel, DnaA levels increase with higher inducer percentage in comparison to WT in minimal media. Right panel shows quantification of cell length in comparison to WT; the maximum drop is observed with M2X. Data points show mean ± SD. A parametric t-test was performed using population mean values (N = 3) to compare values for each measurement. p(<0.0001) ****, p(0.0001)***, p(<0.05)*, ns (non-significant). All samples were blinded n= ~600 cells.

Figure 2. The ability of DnaA to bind ATP and DNA are required for its impact on cell size. A. AlphaFold model of DnaA, domains color coded in blue- domain I, grey- domain II, yellow- domain III, red- domain IV. DnaA truncations show WT and mutant DnaA. Schematic shows empty vector (EV) and merodiploid. (merodiploids have a WT *dnaA* under native promoter and *dnaA* modification under P_{xyl}). Cells were grown overnight in minimal media M2G or M2X (xylose inducer) to exponential phase before serial dilution**,** western sample preparation and microscopy. **B.** Colony forming units showing viability of DnaA mutants in comparison to empty vector EV (*parB*::CFP-*parB* P_{xyl} EV). EV and DnaA mutants show similar growth. **C.** Western blot showing levels of DnaA mutants in comparison to EV. Truncation of domain IV yields 43kDa DnaA. **D.** Super plots showing cell length quantification of EV and DnaA mutants. Small dots represent data points from three independent replicates; large dots represent median values. 3x-DnaA shows ~20% decrease in cell length. Δ*ala* rich region from N-terminus (*parB*::CFP-*parB* P_{xyl}-Δ*ala* N-ter *dnaA*) shows ~15% decrease in cell length. DnaA ATP*K195I (*parB*::CFP-*parB* P_{xyl}-*dnaA* ^{K195I}) and DnaA domain IV truncation (*parB*::CFP-*parB* P_{xyl}-*dnaA* ^{I,II,III}) shows WT cell length ~2.36µm. Data points show mean ± SD. A parametric t test was performed using population mean values (N = 3). p(<0.0001) ****, p(0.0001)***, p(<0.05)*, ns (non-significant). All samples were blinded n=~600 cells.

463 **Figure 3. Chromosome replication remains unchanged in 3x-DnaA cells.** Cells were grown
464 in minimal media M2G or M2X (xylose inducer) with 100μM van overnight to exponential phase
465 before synchrony. Timelapse images were taken after very 5 minutes for DnaN, every 15min for
466 *oriC* and *pleC*. **A.** Assembly of replisome using fluorescently tagged DnaN in WT (*parB*::CFP-
467 *parB dnaN*::*dnaN* mcherry) and 3x-DnaA (*dnaA*::Ω, *parB::cfp-parB,* P_{van} *dnaA, dnaN*::*dnaN*
468 mcherry). In both strains replisome assembles at ~5min represented with red dot. The image is
469 overlayed with CFP *parB* representing *oriC* **B.** Timing of replication initiation was quantified
470 using labelled ParB in WT (*parB*::CFP-*parB*) and 3x-DnaA (*dnaA*::Ω, *parB::cfp-parB,* P_{van} *dnaA*).
471 In both strains, replication initiation occurs at ~15-20min, represented with green dot. **C.**
472 Progression of replication using *parS*(pMT1) near the *pleC* locus in WT (CFP-*parB PvanA*-
473 mCherry-*parB*(pMT1) *parS*(pMT1)-*pleC* and 3x-DnaA (CFP-*parB PvanA*-mCherry-*parB*(pMT1)
474 *parS*(pMT1)-*Pxyl-dnaA*). In both strains a second *pleC* tag appears around ~75min, represented
475 as red dot. Data is representation of three independent experiments. Data points show mean ±
476 SD. A parametric t-test was performed using population mean. p(<0.0001) ****, p(0.0001)***,
477 p(<0.05)*, ns (non-significant). All samples were blinded n=~100 cells.
478
479
480 **Figure 4. 3x-DnaA cells display changes in transcriptional profiles. A.** Cells were grown in
481 minimal media M2G or M2X (xylose inducer) overnight to exponential phase before RNA
482 extraction, sample preparation and microscopy. **A.** (left) RNA-seq data represented as volcano
483 plot (left panel) comparing EV (*parB*::CFP-*parB* P_{xyl} EV) to 3x-DnaA (*parB*::CFP-*parB* P_{xyl}-*dnaA*)
484 represented as dark grey shows 48 genes upregulated and 10 genes downregulated FDR <0.05.
485 (right) Comparison of 3x-DnaA to DnaA K195I (*parB*::CFP-*parB* P_{xyl}-*dnaA* ^{K195I}. **B.** FtsZ levels in
486 WT and 3x-DnaA strain shows comparable levels, FtsZ ~65kDa. **C.** Cell images of EV and
487 merodiploid *ftsZ*, *mraY* and *murD,* scale 2μm. Super plots showing cell length quantification of EV
488 and merodiploid (*parB*::CFP-*parB* P_{xyl}-*ftsZ),* (*parB*::CFP-*parB* P_{xyl}-*mraY),* (*parB*::CFP-*parB* P_{xyl}-
489 *murD).* Small dots represent data points from three independent replicates; large dots represent
490 median values. Induction of *murD* shows 10% decrease in cell length in comparison to EV in
491 minimal media. **D.** Super plots showing cell length quantification of *murD* merodiploid. *murD*
492 overexpression in 3x-DnaA background labelled as 3x-DnaA P_{xyl}-*murD* (*dnaA*::Ω, *parB::cfp-parB,*
493 P_{van} *dnaA,* P_{xyl}-*murD*) results in an additional ~10% decrease in cell length in comparison to 3x-
494 DnaA (*dnaA*::Ω, *parB::cfp-parB,* P_{van} *dnaA).***E.** Growth curves showing induction of *murD* in 3x-
495 DnaA cells (3x-DnaA P_{xyl}-*murD)* leads to a defect on growth rate. Data is representation of three
496 independent experiments. Data points show mean ± SD. A parametric t-test was performed using
497 population mean. p(<0.0001) ****, p(0.0001)***, p(<0.05)*, ns (non-significant). All samples were
498 blinded n=~500 cells.
499
500 **Figure 5. DnaA-ATP regulates the transcription of *murD*. A.** (left) RNA levels of *gcrA* and
501 *murD* in WT (*parB*::CFP-*parB)* in comparison to *gcrA* merodiploid (*parB*::CFP-*parB* P_{xyl}-*gcrA).*
502 *gcrA* RNA levels were increased in *gcrA* merodiploid strain in comparison to WT. *murD* levels
503 were non-significantly changed in comparison to WT. **B.** (right) RNA levels of *dnaA* and *murD* in
504 WT (*parB*::CFP-*parB)* in comparison to *dnaA* merodiploid (*parB*::CFP-*parB* P_{xyl}-*dnaA). dnaA*
505 RNA levels were increased in *dnaA* merodiploid strain in comparison to WT. *murD* levels were
506 significantly increased *dnaA* merodiploid strain. p(<0.0001) ****, p(0.0001)***, p(<0.05)*, ns
507 (non-significant). **C.** Schematic of *murD* operon in *Caulobacter*, with another +1 site upstream of
508 *murD.* Strong DnaA binding box was identified upstream of *mraY.* **D.** EMSA showing DnaA

binding with purified DnaA protein. 200bp upstream of *mraY* containing the DnaA binding box were cloned in a plasmid and used as DNA. Purified DnaA + DNA was incubated with ATP without ATP 30° for 10 minutes. Increasing DnaA concentration in presence of ATP shows a shift, highlighting DnaA binding to the DnaA binding box in the presence of nucleotide.

Figure 6. DnaA modulates cell growth and constriction rates. A. Timelapse phase contrast images of WT (*parB*::CFP-*parB)* and 3x-DnaA (*dnaA*::Ω, *parB::cfp-parB,* P_{van} *dnaA)*. Cells were grown in M2G overnight with inducer 100μM van to exponential phase before synchrony, time-lapse images were taken after very 5 minutes, representative images are shown at 5 min, and then 45 min to 135 minutes post synchrony. scale 2μm. **B.** Phase contrast images showing initial length and initial width and constriction. scale 2μm. The yellow lines represent measures of length or width for each cell. **C.** Super plots showing quantification of rate of constriction in WT and 3x-DnaA. Constriction was significantly faster in 3x-DnaA cells. **D.** Super plots of quantification of rate of elongation shows it is reduced by ~20% in 3x-DnaA cells. Super plot of ratio of rate of constriction over rate of elongation shows a shift in favor of constriction in 3x-DnaA cells. Small dots represent data points from four independent replicates, large dots represent median values (blue,pink,orange,yellow). Each data point is an independent experiment. Data points show mean ± SD. A parametric t-test was performed using population mean values (N = 4) to compare values for each measurement. p(<0.0001) ****, p(0.0001)***, p(<0.05)*, ns (non-significant). All samples were blinded n= ~300 cells.

MATERIALS AND METHODS

Bacterial strains and growth conditions

Strain and plasmid descriptions are listed in the Supplementary Table S2, S3. *Caulobacter crescentus* strains used in this study were derived from NA1000 (wildtype). Plasmids were constructed by cloning PCR products into pNPTS138,pXCHYC-2, pBXMCS-2 vectors [35]. Amplified PCR products were placed in vectors via Gibson or restriction cloning. Plasmids were transformed into DH5α cells and verified through sequencing. In *C. crescentus*, plasmids were transformed via electroporation. *Caulobacter* strains were grown in peptone yeast extract (PYE) or M2 minimal media supplemented with 0.2% glucose (M2G) or 0.2% xylose (M2X). Liquid cultures were re-inoculated overnight in fresh media to grow cells until exponential phase OD_{600} ~ 0.3-0.4 at 30°C under mechanical agitation 200 rpm. Overnight cultures were supplemented with specific antibiotics and inducers. Vanillate 100μM was used to induce the expression of P_{van}, while 0.3% xylose or M2X was used to induce P_{xyl}. Liquid cultures were supplemented with following concentrations of antibiotics: 5μg/ml kanamycin, 25μg/ml spectinomycin, 5μg/ml streptomycin. For PYE plates 25μg/ml kanamycin, 100μg/ml spectinomycin and 5μg/ml streptomycin. To check the impact of chloramphenicol, cerulenin and fosfomycin, 1/10 (2 μg/ml) sub-lethal concentration of chloramphenicol, 0.6μg/ml cerulenin and 5μg/ml fosfomycin was added to liquid culture and left overnight such that the OD is 0.3 next day.

552 **Synchronization**
553 *C.crescentus* cells were synchronized using mini-synchrony protocol to isolate swarmer
554 population [93]. Cells were inoculated in 15ml M2G overnight, to an OD_{600} ~ 0.3. Cultures were
555 supplemented with inducer and antibiotics as noted. Cells were pelleted at 6000 rpm for 10
556 minutes at 4°C in the centrifuge. Cell pellet was resuspended in 900µl of 1X M2 salts and 900µl
557 of Percoll (Sigma-Aldrich) for density gradient. The mixed solution was centrifuged at 11.000rpm
558 for 20minutes, the bottom layer of swarmer cells was isolated and transferred to a fresh tube.
559 Cells were washed twice with ice cold 1X M2 salts, centrifuged at 8000 rpm for 3 minutes at 4°C.
560 Swarmer's were resuspended in M2G to appropriate OD_{600} ~0.2-0.3.
561
562 **Growth assays**
563 *C.cresentus* overnight cultures were grown from freezer stock in M2G or PYE liquid medium were
564 back diluted to reach OD_{600} ~0.1 for growth curves. Early log phase cultures were used for
565 inoculation in 96-well plate in M2G or PYE with relevant inducer. Optical density at 600 nm was
566 monitored every hour at 30°C in a Biotek EPOCH-2 microplate reader with shaking.
567
568 **Microscopy**
569 Cells were grown to an exponential OD_{600} ~0.3. Cells (1µl) were spotted on agar pads (1%
570 agarose in M2G or M2salts). For time-lapses (2µl) cells were spotted on agar pads.
571 Phase contrast and fluorescent images were taken at room temperature using Zeiss Axio
572 Observer 2.1 inverted microscope with AxioCam 506 mono camera (objective: Plan-apochromat
573 100x/1.40 Oil Ph3 M27 [WD=0.17mm]) and Zen Pro software. Samples were blinded for data
574 analysis. To count number of foci, ImageJ (cell counter plugin) was used [94]. Cell size (length and
575 width) was analyzed using ImageJ/FIJI plugin MicrobeJ [67]. Multiple frames were analyzed for cell
576 size analysis, data were presented in Superplots [95].
577
578 **Elongation and constriction**
579 Cells were grown in liquid cultures with inducer overnight to reach early log phase OD_{600} ~0.3 to
580 synchronize. After synchrony cell were resuspended in M2G or M2X with appropriate additives.
581 Cells were then spotted on agar pads (0.1% agar with inducer) for timelapse. Images were taken
582 after every 5 minutes through one cell cycle. MicrobeJ was used to analyze timelapse images as
583 described by [83,96]. Constriction is automatically detected at the positive curvature midcell and
584 manually segmented upon division. Cell width was detected at the site of constriction whereas
585 cell length was calculated at each time point. Cell width was detected at the site of constriction
586 whereas cell length was calculated at each time point. Constriction time was determined by
587 multiplying the number of frames from constriction initiation to division by 5 (images were taken
588 every 5min). The constriction rate was calculated by dividing the cell width at the onset of
589 constriction by the constriction time. Elongation rate calculated by dividing change in length from
590 constriction initiation to division by constriction time.

591
592
593

594 **Immunoblotting**
595 *Caulobacter* mixed population cells were grown to early exponential phase OD_{600} ~0.3 with
596 inducer. The OD_{600} of the incubated cultures was normalized to 0.2. Cells were pelted and
597 resuspended in 40μl of cracking buffer, then boiled for 10 min at 90°C. Samples were stored at -
598 20°C for western blotting. A 12% SDS-PAGE gel was used to separate proteins and then
599 transferred to PVD membrane using iBlot2 (Invitrogen Dry Blotting System). The membrane was
600 blocked with 1XTBS (10mM Tris-HCL, pH8,150mM NaCl, 0.1% Tween-20), 0.1% tween 20
601 (TBST) and 5% non-fat milk at room temperature. The blot was incubated overnight with primary
602 antibody for DnaA (α-DnaA) [97] at a dilution of 1:15,000 for FtsZ (α-FtsZ)[98] at a 1:20,000 dilution
603 in TBST with 5% milk overnight at 4°C. Next day the membrane was washed 3X with TBST and
604 then incubated with secondary antibody (α-Rabbit IgG peroxidase, Sigma-Aldrich) diluted to
605 1:15,000 in TBST with 5% milk at room temperature for 1 hour. The blot was washed 3X with
606 TBST for 5 minutes. To develop the blot, SuperSignal West Pico PLUS Chemiluminescent
607 Substrate (Themo Fisher Scientific) was used and imaged by using ChemiDoc-MP (Bio-Rad). WT
608 DnaA runs at 56kDa, whereas WT FtsZ is 54.1kDa, but it runs at ~65kDa.
609
610 **CFUs for viability assay**
611 *Caulobacter* cells were grown from freezer stocks in minimal media M2G or M2X, it was then
612 reinoculated in fresh media with relevant additives at 30°C 180rpm to reach exponential growth
613 OD_{600} ~0.3. Cells were then normalized to OD_{600} ~0.1. Cultures were serially diluted in a 96-well
614 plate and plated on M2G or M2X plates (0.2% xylose in M2X plates was used as inducer). Plates
615 were incubated at 30°C for 2 days and then imaged using ChemiDoc-MP (Bio-Rad).

616 **RNA-sequencing**
617 *Caulobacter* cells were grown from freezer stocks in minimal media M2G, reinoculated in fresh
618 media M2G or M2X (M2X media to induce the expression of mutants) at 30°C 180rpm to reach
619 exponential growth OD_{600} ~0.3. Total RNA was extracted using hot phenol procedure [99]. After
620 total RNA extraction it was treated with DNase (Invitrogen TURBO DNase) to remove genomic
621 DNA and quantitated using nanodrop (Themo Fisher Scientific NanoDrop One[c]). Samples were
622 then sent to Roy J. Carver Biotechnology Center Sequencing core at UIUC to check RNA integrity
623 through Bioanalyzer, library preparation, sequencing, and data analysis.
624
625 **RT-qPCR**
626 *Caulobacter* cells were grown from freezer stocks in minimal media M2G, reinoculated in fresh
627 media M2G or M2X (M2X media to induce the expression of mutants) at 30°C 180rpm to reach
628 exponential growth OD_{600} ~0.3. Total RNA was extracted using hot phenol procedure [99]. After
629 total RNA extraction it was treated with DNase (Invitrogen TURBO DNase) to remove genomic
630 DNA and quantitated using nanodrop (Themo Fisher Scientific NanoDrop One[c]). cDNA synthesis
631 and Rt-qPCR was performed using Luna universal one-step RT-qPCR kit. Final concentration of
632 RNA was 10ng for each reaction. To quantify transcription *ruvA* (*CCNA_03345*) was used as an
633 endogenous control, with the following primers: 5′-cgagtgaggaagccgtagag-3′ and 5′-
634 gaccctgttgcacatcgag-3′ [100].
635

636 **EMSA**

637 EMSA experiments were performed as described previously. DNA fragment was incubated with
638 purified DnaA protein in EMSA buffer containing 20mM HEPES,10mM MgAc, 60mM NaCl, 5%
639 glycerol, 0.1mg/ml bovine serum albumin and 3mM ATP or without ATP. DNA fragment and
640 purified DnaA was incubated in EMSA buffer at 30° for 10 minutes. Samples were run on 2% TBE
641 gel in TBE buffer at 90 V for 6 hours in 4°. DNA was visualized by ethidium bromide staining.

642 **REFERENCES**
643

644 1. Westfall, C.S., and Levin, P.A. (2017). Bacterial Cell Size: Multifactorial and Multifaceted.
645 Annu Rev Microbiol *71*, 499-517. 10.1146/annurev-micro-090816-093803.
646 2. Wang, J.D., and Levin, P.A. (2009). Metabolism, cell growth and the bacterial cell cycle.
647 Nat Rev Microbiol *7*, 822-827. 10.1038/nrmicro2202.
648 3. Hansen, F.G., and Atlung, T. (2018). The DnaA Tale. Front Microbiol *9*, 319.
649 10.3389/fmicb.2018.00319.
650 4. Kohiyama, M. (2020). Research on DnaA in the early days. Res Microbiol *171*, 287-289.
651 10.1016/j.resmic.2020.11.004.
652 5. Bramhill, D., and Kornberg, A. (1988). A model for initiation at origins of DNA replication.
653 Cell *54*, 915-918. 10.1016/0092-8674(88)90102-x.
654 6. Katayama, T., Kubota, T., Kurokawa, K., Crooke, E., and Sekimizu, K. (1998). The
655 initiator function of DnaA protein is negatively regulated by the sliding clamp of the E. coli
656 chromosomal replicase. Cell *94*, 61-71. 10.1016/s0092-8674(00)81222-2.
657 7. Su'etsugu, M., Shimuta, T.R., Ishida, T., Kawakami, H., and Katayama, T. (2005). Protein
658 associations in DnaA-ATP hydrolysis mediated by the Hda-replicase clamp complex. J Biol
659 Chem *280*, 6528-6536. 10.1074/jbc.M412060200.
660 8. Menikpurage, I.P., Woo, K., and Mera, P.E. (2021). Transcriptional Activity of the
661 Bacterial Replication Initiator DnaA. Front Microbiol *12*, 662317. 10.3389/fmicb.2021.662317.
662 9. Messer, W., and Weigel, C. (1997). DnaA initiator--also a transcription factor. Mol
663 Microbiol *24*, 1-6. 10.1046/j.1365-2958.1997.3171678.x.
664 10. Goranov, A.I., Katz, L., Breier, A.M., Burge, C.B., and Grossman, A.D. (2005). A
665 transcriptional response to replication status mediated by the conserved bacterial replication
666 protein DnaA. Proc Natl Acad Sci U S A *102*, 12932-12937. 10.1073/pnas.0506174102.
667 11. Breier, A.M., and Grossman, A.D. (2009). Dynamic association of the replication initiator
668 and transcription factor DnaA with the Bacillus subtilis chromosome during replication stress. J
669 Bacteriol *191*, 486-493. 10.1128/jb.01294-08.
670 12. Mizushima, T., Sasaki, S., Ohishi, H., Kobayashi, M., Katayama, T., Miki, T., Maeda, M.,
671 and Sekimizu, K. (1996). Molecular design of inhibitors of in vitro oriC DNA replication based on
672 the potential to block the ATP binding of DnaA protein. J Biol Chem *271*, 25178-25183.
673 10.1074/jbc.271.41.25178.
674 13. Sekimizu, K., Bramhill, D., and Kornberg, A. (1987). ATP activates dnaA protein in
675 initiating replication of plasmids bearing the origin of the E. coli chromosome. Cell *50*, 259-265.
676 10.1016/0092-8674(87)90221-2.
677 14. Fernandez-Fernandez, C., Gonzalez, D., and Collier, J. (2011). Regulation of the Activity
678 of the Dual-Function DnaA Protein in Caulobacter crescentus. PLOS ONE *6*, e26028.
679 10.1371/journal.pone.0026028.
680 15. Speck, C., Weigel, C., and Messer, W. (1999). ATP- and ADP-dnaA protein, a molecular
681 switch in gene regulation. EMBO J *18*, 6169-6176. 10.1093/emboj/18.21.6169.
682 16. Olliver, A., Saggioro, C., Herrick, J., and Sclavi, B. (2010). DnaA-ATP acts as a molecular
683 switch to control levels of ribonucleotide reductase expression in Escherichia coli. Mol Microbiol
684 *76*, 1555-1571. 10.1111/j.1365-2958.2010.07185.x.
685 17. Haeusser, D.P., and Levin, P.A. (2008). The great divide: coordinating cell cycle events
686 during bacterial growth and division. Current Opinion in Microbiology *11*, 94-99.
687 https://doi.org/10.1016/j.mib.2008.02.008.
688 18. Garde, S., Chodisetti Pavan, K., and Reddy, M. (2021). Peptidoglycan: Structure,
689 Synthesis, and Regulation. EcoSal Plus *9*. 10.1128/ecosalplus.ESP-0010-2020.

690 19. Barreteau, H., Kovač, A., Boniface, A., Sova, M., Gobec, S., and Blanot, D. (2008).
691 Cytoplasmic steps of peptidoglycan biosynthesis. FEMS microbiology reviews *32*, 168-207.
692 20. Vollmer, W., Blanot, D., and De Pedro, M.A. (2008). Peptidoglycan structure and
693 architecture. FEMS microbiology reviews *32*, 149-167.
694 21. Höltje, J.-V. (1998). Growth of the stress-bearing and shape-maintaining murein sacculus
695 of Escherichia coli. Microbiology and molecular biology reviews *62*, 181-203.
696 22. Cava, F., Kuru, E., Brun, Y.V., and de Pedro, M.A. (2013). Modes of cell wall growth
697 differentiation in rod-shaped bacteria. Current Opinion in Microbiology *16*, 731-737.
698 https://doi.org/10.1016/j.mib.2013.09.004.
699 23. Shaevitz, J.W., and Gitai, Z. (2010). The structure and function of bacterial actin
700 homologs. Cold Spring Harbor perspectives in biology *2*, a000364.
701 24. Aaron, M., Charbon, G., Lam, H., Schwarz, H., Vollmer, W., and Jacobs-Wagner, C.
702 (2007). The tubulin homologue FtsZ contributes to cell elongation by guiding cell wall precursor
703 synthesis in Caulobacter crescentus. Molecular Microbiology *64*, 938-952.
704 https://doi.org/10.1111/j.1365-2958.2007.05720.x.
705 25. Govers, S.K., and Jacobs-Wagner, C. (2020). Caulobacter crescentus: model system
706 extraordinaire. Curr Biol *30*, R1151-r1158. 10.1016/j.cub.2020.07.033.
707 26. Campos, M., Surovtsev, I.V., Kato, S., Paintdakhi, A., Beltran, B., Ebmeier, S.E., and
708 Jacobs-Wagner, C. (2014). A constant size extension drives bacterial cell size homeostasis.
709 Cell *159*, 1433-1446. 10.1016/j.cell.2014.11.022.
710 27. Banerjee, S., Lo, K., Daddysman, M.K., Selewa, A., Kuntz, T., Dinner, A.R., and Scherer,
711 N.F. (2017). Biphasic growth dynamics control cell division in Caulobacter crescentus. Nat
712 Microbiol *2*, 17116. 10.1038/nmicrobiol.2017.116.
713 28. Lambert, A., Vanhecke, A., Archetti, A., Holden, S., Schaber, F., Pincus, Z., Laub, M.T.,
714 Goley, E., and Manley, S. (2018). Constriction Rate Modulation Can Drive Cell Size Control and
715 Homeostasis in C. crescentus. iScience *4*, 180-189. https://doi.org/10.1016/j.isci.2018.05.020.
716 29. Barrows, J.M., and Goley, E.D. (2023). Synchronized Swarmers and Sticky Stalks:
717 Caulobacter crescentus as a Model for Bacterial Cell Biology. J Bacteriol *205*, e0038422.
718 10.1128/jb.00384-22.
719 30. Evinger, M., and Agabian, N. (1977). Envelope-associated nucleoid from Caulobacter
720 crescentus stalked and swarmer cells. J Bacteriol *132*, 294-301. 10.1128/jb.132.1.294-
721 301.1977.
722 31. Schrader, J.M., and Shapiro, L. (2015). Synchronization of Caulobacter crescentus for
723 investigation of the bacterial cell cycle. J Vis Exp. 10.3791/52633.
724 32. Stove, J.L., and Stanier, R.Y. (1962). Cellular Differentiation in Stalked Bacteria. Nature
725 *196*, 1189-1192. 10.1038/1961189a0.
726 33. Ardissone, S., Fumeaux, C., Berge, M., Beaussart, A., Theraulaz, L., Radhakrishnan,
727 S.K., Dufrene, Y.F., and Viollier, P.H. (2014). Cell cycle constraints on capsulation and
728 bacteriophage susceptibility. Elife *3*. 10.7554/eLife.03587.
729 34. Marczynski, G.T. (1999). Chromosome methylation and measurement of faithful, once
730 and only once per cell cycle chromosome replication in Caulobacter crescentus. J Bacteriol *181*,
731 1984-1993. 10.1128/JB.181.7.1984-1993.1999.
732 35. Thanbichler, M., Iniesta, A.A., and Shapiro, L. (2007). A comprehensive set of plasmids
733 for vanillate- and xylose-inducible gene expression in Caulobacter crescentus. Nucleic Acids
734 Research *35*, e137-e137. 10.1093/nar/gkm818.
735 36. Schaechter, M., Maaløe, O., and Kjeldgaard, N.O. (1958). Dependency on medium and
736 temperature of cell size and chemical composition during balanced growth of Salmonella
737 typhimurium. Microbiology *19*, 592-606.

37. Toro, E., Hong, S.H., McAdams, H.H., and Shapiro, L. (2008). Caulobacter requires a dedicated mechanism to initiate chromosome segregation. Proc Natl Acad Sci U S A *105*, 15435-15440. 10.1073/pnas.0807448105.
38. Thanbichler, M., and Shapiro, L. (2006). MipZ, a Spatial Regulator Coordinating Chromosome Segregation with Cell Division in Caulobacter. Cell *126*, 147-162. 10.1016/j.cell.2006.05.038.
39. Ng, T.W., Ojkic, N., Serbanescu, D., and Banerjee, S. (2024). Differential growth regulates asymmetric size partitioning in Caulobacter crescentus. Life Science Alliance *7*, e202402591. 10.26508/lsa.202402591.
40. Glenn, S., Fragasso, A., Lin, W.-H., Papagiannakis, A., Kato, S., and Jacobs-Wagner, C. (2024). Coupling of cell growth modulation to asymmetric division and cell cycle regulation in Caulobacter crescentus. Proceedings of the National Academy of Sciences *121*, e2406397121. doi:10.1073/pnas.2406397121.
41. Felletti, M., Omnus, D.J., and Jonas, K. (2019). Regulation of the replication initiator DnaA in Caulobacter crescentus. Biochim Biophys Acta Gene Regul Mech *1862*, 697-705. 10.1016/j.bbagrm.2018.01.004.
42. Katayama, T., Ozaki, S., Keyamura, K., and Fujimitsu, K. (2010). Regulation of the replication cycle: conserved and diverse regulatory systems for DnaA and oriC. Nature Reviews Microbiology *8*, 163-170.
43. Stephens, C., Christen, B., Watanabe, K., Fuchs, T., and Jenal, U. (2007). Regulation of d-Xylose Metabolism in Caulobacter crescentus by a LacI-Type Repressor. Journal of Bacteriology *189*, 8828-8834. doi:10.1128/jb.01342-07.
44. Basan, M., Zhu, M., Dai, X., Warren, M., Sevin, D., Wang, Y.P., and Hwa, T. (2015). Inflating bacterial cells by increased protein synthesis. Mol Syst Biol *11*, 836. 10.15252/msb.20156178.
45. Vadia, S., Tse, J.L., Lucena, R., Yang, Z., Kellogg, D.R., Wang, J.D., and Levin, P.A. (2017). Fatty Acid Availability Sets Cell Envelope Capacity and Dictates Microbial Cell Size. Curr Biol *27*, 1757-1767.e1755. 10.1016/j.cub.2017.05.076.
46. Felletti, M., Romilly, C., Wagner, E.G.H., and Jonas, K. (2021). A nascent polypeptide sequence modulates DnaA translation elongation in response to nutrient availability. Elife *10*. 10.7554/eLife.71611.
47. Mizushima, T., Takaki, T., Kubota, T., Tsuchiya, T., Miki, T., Katayama, T., and Sekimizu, K. (1998). Site-directed mutational analysis for the ATP binding of DnaA protein. Functions of two conserved amino acids (Lys-178 and Asp-235) located in the ATP-binding domain of DnaA protein in vitro and in vivo. J Biol Chem *273*, 20847-20851. 10.1074/jbc.273.33.20847.
48. Leonard, A.C., and Grimwade, J.E. (2011). Regulation of DnaA assembly and activity: taking directions from the genome. Annu Rev Microbiol *65*, 19-35.
49. Jensen, R.B., Wang, S.C., and Shapiro, L. (2001). A moving DNA replication factory in Caulobacter crescentus. EMBO J *20*, 4952-4963. 10.1093/emboj/20.17.4952.
50. Collier, J., and Shapiro, L. (2009). Feedback control of DnaA-mediated replication initiation by replisome-associated HdaA protein in Caulobacter. J Bacteriol *191*, 5706-5716. 10.1128/JB.00525-09.
51. Schwartz, M.A., and Shapiro, L. (2011). An SMC ATPase mutant disrupts chromosome segregation in Caulobacter. Molecular microbiology *82*, 1359-1374.
52. Messer, W., and Weigel, C. (1997). DnaA initiator—also a transcription factor. Molecular microbiology *24*, 1-6.
53. Washington, T.A., Smith, J.L., and Grossman, A.D. (2017). Genetic networks controlled by the bacterial replication initiator and transcription factor DnaA in Bacillus subtilis. Molecular microbiology *106*, 109-128.

54. Hottes, A.K., Shapiro, L., and McAdams, H.H. (2005). DnaA coordinates replication initiation and cell cycle transcription in Caulobacter crescentus. Molecular Microbiology *58*, 1340-1353. https://doi.org/10.1111/j.1365-2958.2005.04912.x.
55. Hottes, A.K., Shapiro, L., and McAdams, H.H. (2005). DnaA coordinates replication initiation and cell cycle transcription in Caulobacter crescentus. Mol Microbiol *58*, 1340-1353. 10.1111/j.1365-2958.2005.04912.x.
56. Collier, J., Murray, S.R., and Shapiro, L. (2006). DnaA couples DNA replication and the expression of two cell cycle master regulators. The EMBO Journal *25*, 346-356-356. https://doi.org/10.1038/sj.emboj.7600927.
57. Sackett, M.J., Kelly, A.J., and Brun, Y.V. (1998). Ordered expression of ftsQA and ftsZ during the Caulobacter crescentus cell cycle. Mol Microbiol *28*, 421-434. 10.1046/j.1365-2958.1998.00753.x.
58. Si, F., Le Treut, G., Sauls, J.T., Vadia, S., Levin, P.A., and Jun, S. (2019). Mechanistic origin of cell-size control and homeostasis in bacteria. Current Biology *29*, 1760-1770. e1767.
59. Xu, X., Cui, J., Xu, H., Sun, J., Yuan, X., Jia, Y., Luan, G., and Lu, X. (2026). FtsZ overexpression-induced cell miniaturization reshapes photosynthesis and enhances transformation efficiency in Synechococcus elongatus PCC 7942. Algal Research *93*, 104473. https://doi.org/10.1016/j.algal.2025.104473.
60. Goley, E.D., Dye, N.A., Werner, J.N., Gitai, Z., and Shapiro, L. (2010). Imaging-Based Identification of a Critical Regulator of FtsZ Protofilament Curvature in Caulobacter. Molecular Cell *39*, 975-987. https://doi.org/10.1016/j.molcel.2010.08.027.
61. Typas, A., Banzhaf, M., Gross, C.A., and Vollmer, W. (2012). From the regulation of peptidoglycan synthesis to bacterial growth and morphology. Nature Reviews Microbiology *10*, 123-136. 10.1038/nrmicro2677.
62. Ikeda, M., Wachi, M., Jung, H.K., Ishino, F., and Matsuhashi, M. (1991). The Escherichia coli mraY gene encoding UDP-N-acetylmuramoyl-pentapeptide: undecaprenyl-phosphate phospho-N-acetylmuramoyl-pentapeptide transferase. J Bacteriol *173*, 1021-1026. 10.1128/jb.173.3.1021-1026.1991.
63. Karp, P.D., Billington, R., Caspi, R., Fulcher, C.A., Latendresse, M., Kothari, A., Keseler, I.M., Krummenacker, M., Midford, P.E., Ong, Q., et al. (2017). The BioCyc collection of microbial genomes and metabolic pathways. Briefings in Bioinformatics *20*, 1085-1093. 10.1093/bib/bbx085.
64. Schrader, J.M., Li, G.-W., Childers, W.S., Perez, A.M., Weissman, J.S., Shapiro, L., and McAdams, H.H. (2016). Dynamic translation regulation in Caulobacter cell cycle control. Proceedings of the National Academy of Sciences *113*, E6859-E6867.
65. Ozaki, S., Noguchi, Y., Hayashi, Y., Miyazaki, E., and Katayama, T. (2012). Differentiation of the DnaA-oriC subcomplex for DNA unwinding in a replication initiation complex. J Biol Chem *287*, 37458-37471. 10.1074/jbc.M112.372052.
66. Schindelin, J., Arganda-Carreras, I., Frise, E., Kaynig, V., Longair, M., Pietzsch, T., Preibisch, S., Rueden, C., Saalfeld, S., Schmid, B., et al. (2012). Fiji: an open-source platform for biological-image analysis. Nature Methods *9*, 676-682. 10.1038/nmeth.2019.
67. Ducret, A., Quardokus, E.M., and Brun, Y.V. (2016). MicrobeJ, a tool for high throughput bacterial cell detection and quantitative analysis. Nat Microbiol *1*, 16077. 10.1038/nmicrobiol.2016.77.
68. Lambert, A., Vanhecke, A., Archetti, A., Holden, S., Schaber, F., Pincus, Z., Laub, M.T., Goley, E., and Manley, S. (2018). Constriction Rate Modulation Can Drive Cell Size Control and Homeostasis in C. crescentus. iScience *4*, 180-189. 10.1016/j.isci.2018.05.020.
69. Lariviere, P.J., Mahone, C.R., Santiago-Collazo, G., Howell, M., Daitch, A.K., Zeinert, R., Chien, P., Brown, P.J.B., and Goley, E.D. (2019). An Essential Regulator of Bacterial Division

838 Links FtsZ to Cell Wall Synthase Activation. Curr Biol *29*, 1460-1470.e1464.
839 10.1016/j.cub.2019.03.066.
840 70. Lariviere, P.J., Szwedziak, P., Mahone, C.R., Löwe, J., and Goley, E.D. (2018). FzlA, an
841 essential regulator of FtsZ filament curvature, controls constriction rate during Caulobacter
842 division. Molecular Microbiology *107*, 180-197. https://doi.org/10.1111/mmi.13876.
843 71. Woldringh, C.L., Grover, N.B., Rosenberger, R.F., and Zaritsky, A. (1980). Dimensional
844 rearrangement of rod-shaped bacteria following nutritional shift-up. II. Experiments with
845 Escherichia coli B/r. J Theor Biol *86*, 441-454. 10.1016/0022-5193(80)90344-6.
846 72. Schaechter, M., Maaloe, O., and Kjeldgaard, N.O. (1958). Dependency on medium and
847 temperature of cell size and chemical composition during balanced grown of Salmonella
848 typhimurium. J Gen Microbiol *19*, 592-606. 10.1099/00221287-19-3-592.
849 73. Sargent, M.G. (1975). Control of cell length in Bacillus subtilis. J Bacteriol *123*, 7-19.
850 10.1128/jb.123.1.7-19.1975.
851 74. Weart, R.B., Lee, A.H., Chien, A.C., Haeusser, D.P., Hill, N.S., and Levin, P.A. (2007). A
852 metabolic sensor governing cell size in bacteria. Cell *130*, 335-347. 10.1016/j.cell.2007.05.043.
853 75. Donachie, W.D., Begg, K.J., and Vicente, M. (1976). Cell length, cell growth and cell
854 division. Nature *264*, 328-333. 10.1038/264328a0.
855 76. Azam, M.A., and Jupudi, S. (2020). MurD inhibitors as antibacterial agents: a review.
856 Chemical Papers *74*, 1697-1708. 10.1007/s11696-020-01057-w.
857 77. Sink, R., Barreteau, H., Patin, D., Mengin-Lecreulx, D., Gobec, S., and Blanot, D. (2013).
858 MurD enzymes: some recent developments. Biomol Concepts *4*, 539-556. 10.1515/bmc-2013-
859 0024.
860 78. Daitch, A.K., and Goley, E.D. (2020). Uncovering Unappreciated Activities and Niche
861 Functions of Bacterial Cell Wall Enzymes. Current Biology *30*, R1170-R1175.
862 https://doi.org/10.1016/j.cub.2020.07.004.
863 79. Sun, Y., Hürlimann, S., and Garner, E. (2023). Growth rate is modulated by monitoring
864 cell wall precursors in Bacillus subtilis. Nature Microbiology *8*, 469-480. 10.1038/s41564-023-
865 01329-7.
866 80. Marmont, L.S., Orta, A.K., Baileeves, B.W.A., Sychantha, D., Fernández-Galliano, A., Li,
867 Y.E., Greene, N.G., Corey, R.A., Stansfeld, P.J., Clemons, W.M., and Bernhardt, T.G. (2024).
868 Synthesis of lipid-linked precursors of the bacterial cell wall is governed by a feedback control
869 mechanism in Pseudomonas aeruginosa. Nature Microbiology *9*, 763-775. 10.1038/s41564-
870 024-01603-2.
871 81. Monteiro, J.M., Pereira, A.R., Reichmann, N.T., Saraiva, B.M., Fernandes, P.B., Veiga,
872 H., Tavares, A.C., Santos, M., Ferreira, M.T., and Macário, V. (2018). Peptidoglycan synthesis
873 drives an FtsZ-treadmilling-independent step of cytokinesis. Nature *554*, 528-532.
874 82. Schoenemann, K.M., and Margolin, W. (2017). Bacterial Division: FtsZ Treadmills to
875 Build a Beautiful Wall. Current Biology *27*, R301-R303.
876 https://doi.org/10.1016/j.cub.2017.03.019.
877 83. Mahone, C.R., Payne, I.P., Lyu, Z., McCausland, J.W., Barrows, J.M., Xiao, J., Yang, X.,
878 and Goley, E.D. (2024). Integration of cell wall synthesis and chromosome segregation during
879 cell division in Caulobacter. J Cell Biol *223*. 10.1083/jcb.202211026.
880 84. Krusenstjerna, A.C., Saylor, T.C., Arnold, W.K., Tucker, J.S., and Stevenson, B. (2023).
881 Borrelia burgdorferi DnaA and the Nucleoid-Associated Protein EbfC Coordinate Expression of
882 the dnaX-ebfC Operon. J Bacteriol *205*, e0039622. 10.1128/jb.00396-22.
883 85. Washington, T.A., Smith, J.L., and Grossman, A.D. (2017). Genetic networks controlled
884 by the bacterial replication initiator and transcription factor DnaA in Bacillus subtilis. Mol
885 Microbiol *106*, 109-128. 10.1111/mmi.13755.
886 86. Jutras, B.L., Bowman, A., Brissette, C.A., Adams, C.A., Verma, A., Chenail, A.M., and
887 Stevenson, B. (2012). EbfC (YbaB) is a new type of bacterial nucleoid-associated protein and a

global regulator of gene expression in the Lyme disease spirochete. J Bacteriol *194*, 3395-3406. 10.1128/JB.00252-12.
87. Krusenstjerna, A.C., Jusufovic, N., Saylor, T.C., and Stevenson, B. (2024). DnaA modulates the gene expression and morphology of the Lyme disease spirochete. bioRxiv. 10.1101/2024.06.08.598065.
88. Kopytova, D., Popova, V., Kurshakova, M., Shidlovskii, Y., Nabirochkina, E., Brechalov, A., Georgiev, G., and Georgieva, S. (2016). ORC interacts with THSC/TREX-2 and its subunits promote Nxf1 association with mRNP and mRNA export in Drosophila. Nucleic acids research *44*, 4920-4933.
89. Scholefield, G., Veening, J.W., and Murray, H. (2011). DnaA and ORC: more than DNA replication initiators. Trends Cell Biol *21*, 188-194. 10.1016/j.tcb.2010.10.006.
90. Sasaki, T., and Gilbert, D.M. (2007). The many faces of the origin recognition complex. Current opinion in cell biology *19*, 337-343.
91. Chesnokov, I.N., Chesnokova, O.N., and Botchan, M. (2003). A cytokinetic function of Drosophila ORC6 protein resides in a domain distinct from its replication activity. Proceedings of the National Academy of Sciences *100*, 9150-9155. doi:10.1073/pnas.1633580100.
92. Lin, Y.-C., Liu, D., Chakraborty, A., Macias, V., Brister, E., Sonalkar, J., Shen, L., Mitra, J., Ha, T., Kajdacsy-Balla, A., et al. (2023). DNA Damage-Induced, S-Phase Specific Phosphorylation of Orc6 is Critical for the Maintenance of Genome Stability. Molecular and cellular biology *43*, 1-14. 10.1080/10985549.2023.2196204.
93. Tsai, J.-W., and Alley, M.R.K. (2001). Proteolysis of the Caulobacter McpA Chemoreceptor Is Cell Cycle Regulated by a ClpX-Dependent Pathway. Journal of Bacteriology *183*, 5001 - 5007.
94. Schindelin, J., Arganda-Carreras, I., Frise, E., Kaynig, V., Longair, M., Pietzsch, T., Preibisch, S., Rueden, C., Saalfeld, S., and Schmid, B. (2012). Fiji: an open-source platform for biological-image analysis. Nature methods *9*, 676-682.
95. Lord, S.J., Velle, K.B., Mullins, R.D., and Fritz-Laylin, L.K. (2020). SuperPlots: Communicating reproducibility and variability in cell biology. Journal of Cell Biology *219*. 10.1083/jcb.202001064.
96. Lariviere, P.J., Szwedziak, P., Mahone, C.R., Löwe, J., and Goley, E.D. (2018). FzlA, an essential regulator of FtsZ filament curvature, controls constriction rate during Caulobacter division. Mol Microbiol *107*, 180-197. 10.1111/mmi.13876.
97. Mera, P.E., Kalogeraki, V.S., and Shapiro, L. (2014). Replication initiator DnaA binds at the Caulobacter centromere and enables chromosome segregation. Proceedings of the National Academy of Sciences *111*, 16100-16105.
98. Sundararajan, K., Miguel, A., Desmarais, S.M., Meier, E.L., Casey Huang, K., and Goley, E.D. (2015). The bacterial tubulin FtsZ requires its intrinsically disordered linker to direct robust cell wall construction. Nature Communications *6*, 7281. 10.1038/ncomms8281.
99. Aiba, H., Adhya, S., and de Crombrugghe, B. (1981). Evidence for two functional gal promoters in intact Escherichia coli cells. Journal of Biological Chemistry *256*, 11905-11910.
100. Boutte, C.C., and Crosson, S. (2011). The complex logic of stringent response regulation in Caulobacter crescentus: starvation signalling in an oligotrophic environment. Molecular Microbiology *80*, 695-714. https://doi.org/10.1111/j.1365-2958.2011.07602.x.

Figure 1

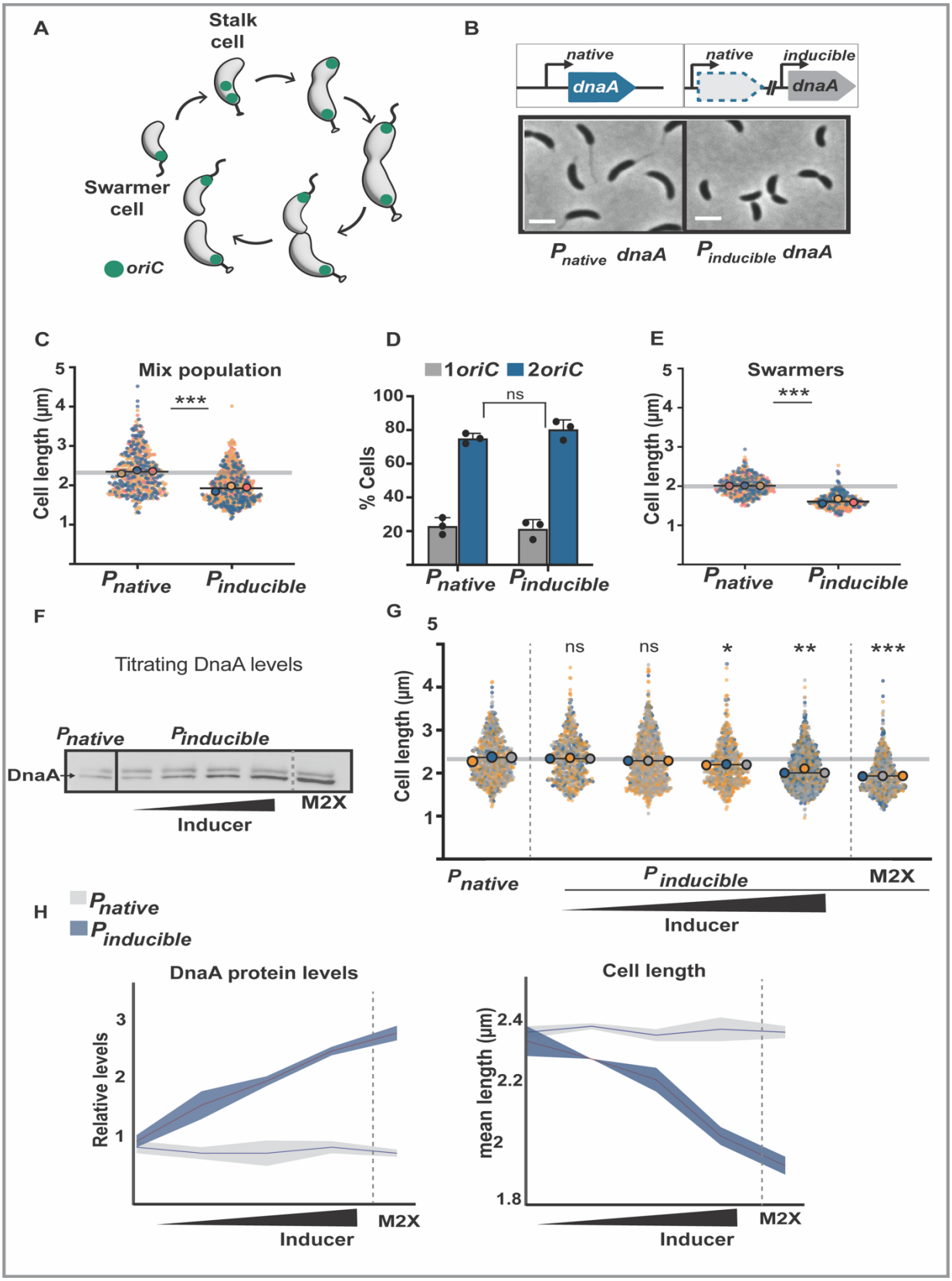
A
Stalk cell
Swarmer cell
oriC
B
native
dnaA
native
inducible
dnaA
P native dnaA
P inducible dnaA
C
Mix population
Cell length (µm)
***
P native
P inducible
D
1oriC
2oriC
% Cells
ns
P native
P inducible
E
Swarmers
Cell length (µm)
***
P native
P inducible
F
Titrating DnaA levels
P native
P inducible
DnaA
M2X
Inducer
G
Cell length (µm)
ns
ns
*
**
***
P native
P inducible
M2X
Inducer
H
P native
P inducible
DnaA protein levels
Relative levels
M2X
Inducer
Cell length
mean length (µm)
M2X
Inducer

Figure 2

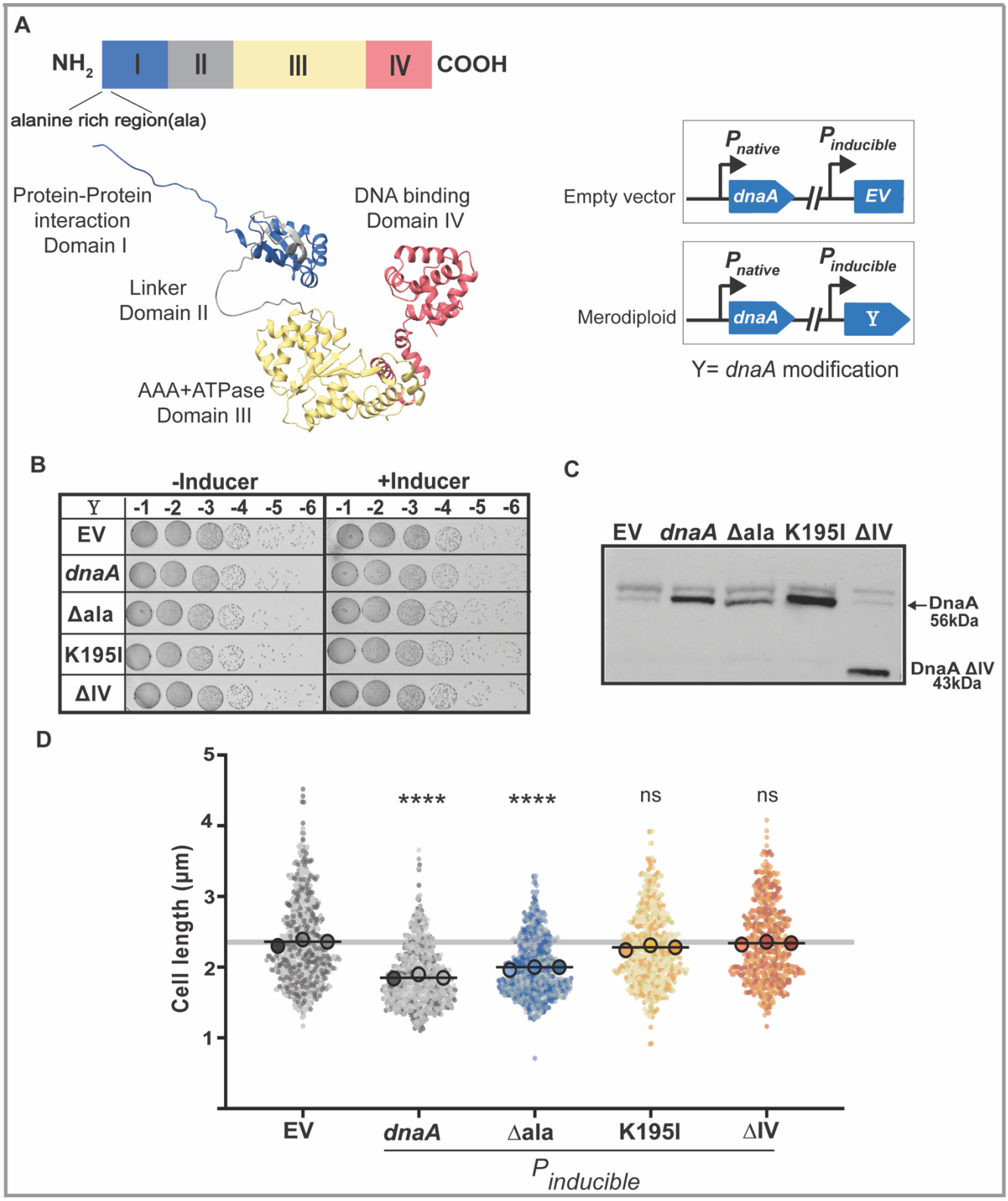
A
NH2
I
II
III
IV
COOH
alanine rich region(ala)
Protein-Protein interaction Domain I
Linker Domain II
AAA+ATPase Domain III
DNA binding Domain IV
Empty vector
Merodiploid
Pnative
Pinducible
dnaA
EV
Y
Y= dnaA modification
B
-Inducer
+Inducer
Y
-1 -2 -3 -4 -5 -6
EV
dnaA
Δala
K195I
ΔIV
C
EV dnaA Δala K195I ΔIV
DnaA 56kDa
DnaA ΔIV 43kDa
D
Cell length (µm)
****
****
ns
ns
EV
dnaA
Δala
K195I
ΔIV
Pinducible

Figure 3

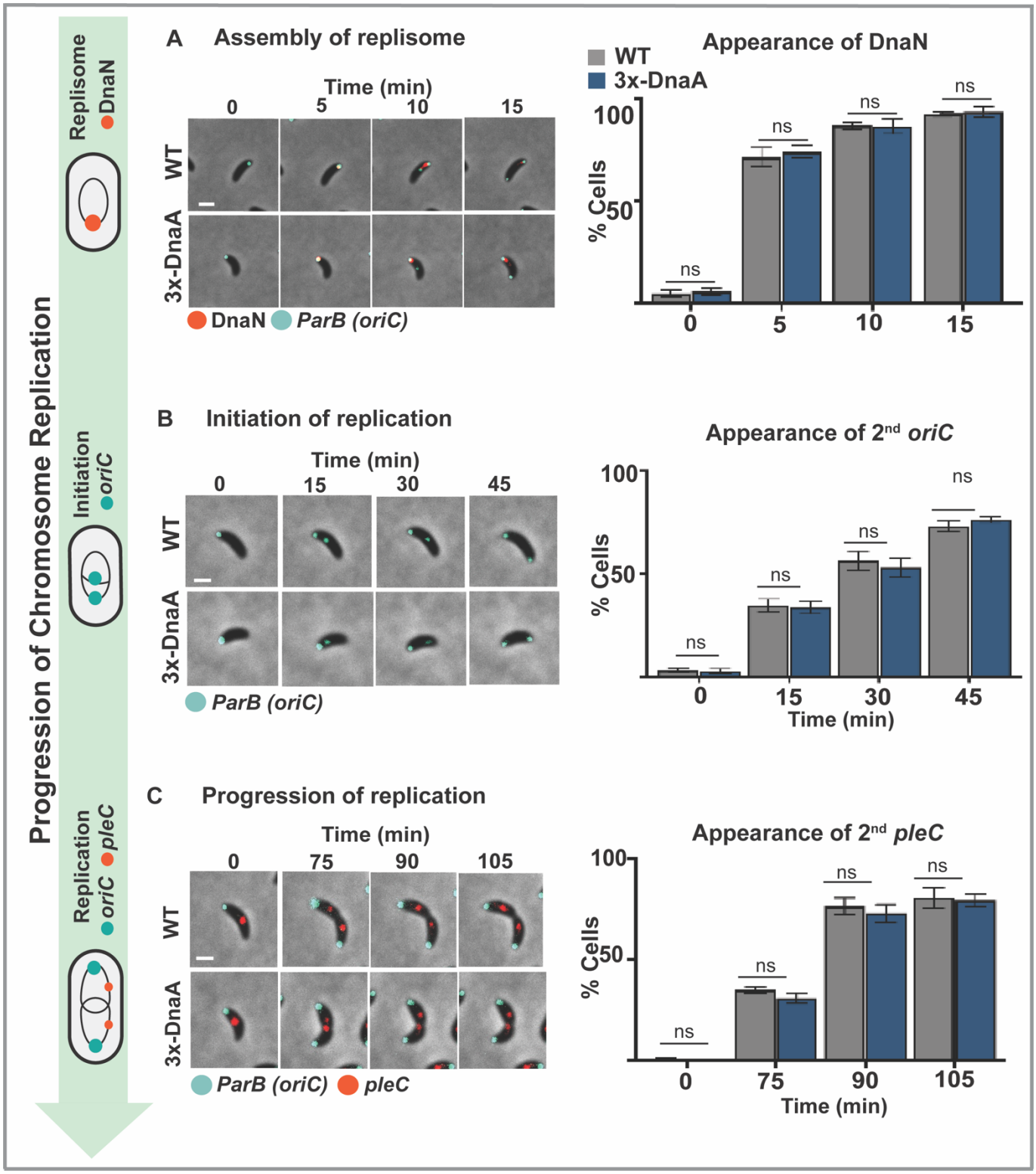
Progression of Chromosome Replication
Replisome
DnaN
Initiation
oriC
Replication
oriC
pleC
A
Assembly of replisome
Time (min)
0
5
10
15
WT
3x-DnaA
DnaN
ParB (oriC)
Appearance of DnaN
WT
3x-DnaA
% Cells
100
50
ns
B
Initiation of replication
Time (min)
0
15
30
45
ParB (oriC)
Appearance of 2nd oriC
Time (min)
C
Progression of replication
Time (min)
0
75
90
105
ParB (oriC)
pleC
Appearance of 2nd pleC
Time (min)

Figure 4

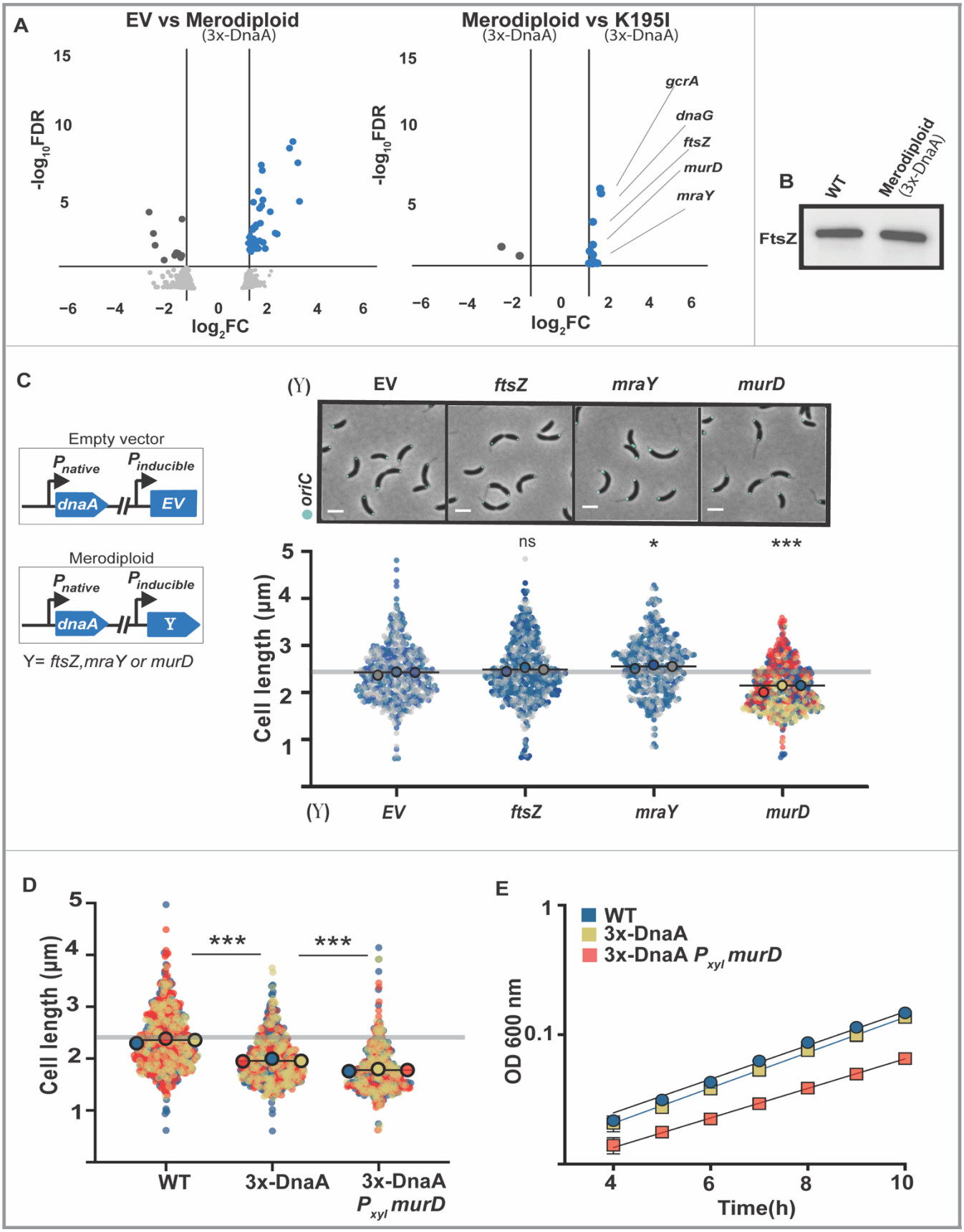
A
EV vs Merodiploid
(3x-DnaA)
Merodiploid vs K195I
(3x-DnaA)
(3x-DnaA)
-log10FDR
log2FC
gcrA
dnaG
ftsZ
murD
mraY
B
WT
Merodiploid
(3x-DnaA)
FtsZ
C
Empty vector
Pnative
Pinducible
dnaA
EV
Merodiploid
Y
Y= ftsZ,mraY or murD
(Y)
EV
ftsZ
mraY
murD
oriC
ns
*
***
Cell length (µm)
D
***
***
WT
3x-DnaA
3x-DnaA
Pxyl murD
E
WT
3x-DnaA
3x-DnaA Pxyl murD
OD 600 nm
Time(h)

Figure 5

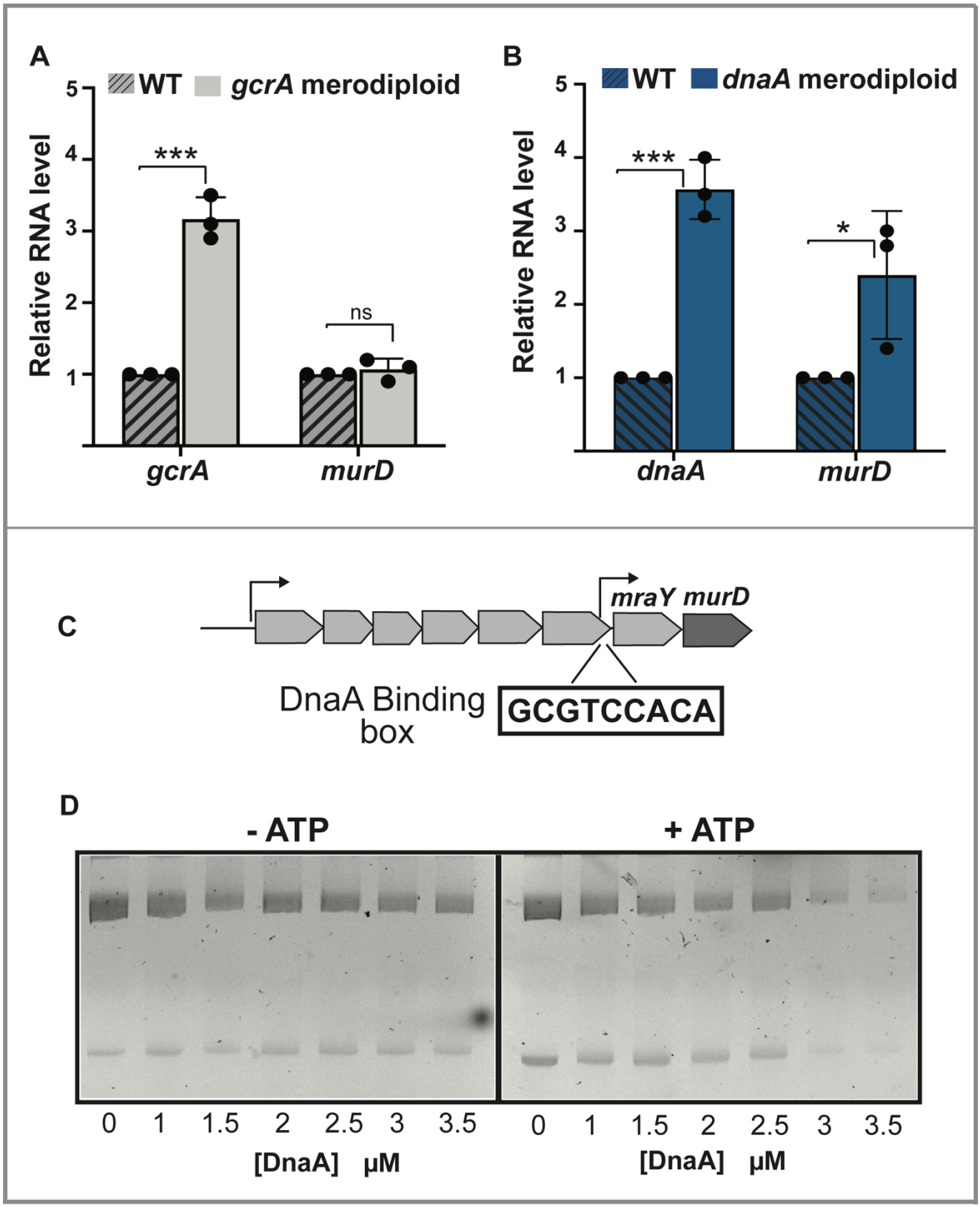
A
WT
gcrA merodiploid
Relative RNA level
5
4
3
2
1
***
ns
gcrA
murD
B
WT
dnaA merodiploid
Relative RNA level
5
4
3
2
1
***
*
dnaA
murD
C
mraY murD
DnaA Binding box
GCGTCCACA
D
- ATP
+ ATP
0 1 1.5 2 2.5 3 3.5
[DnaA] µM
0 1 1.5 2 2.5 3 3.5
[DnaA] µM

Figure 6

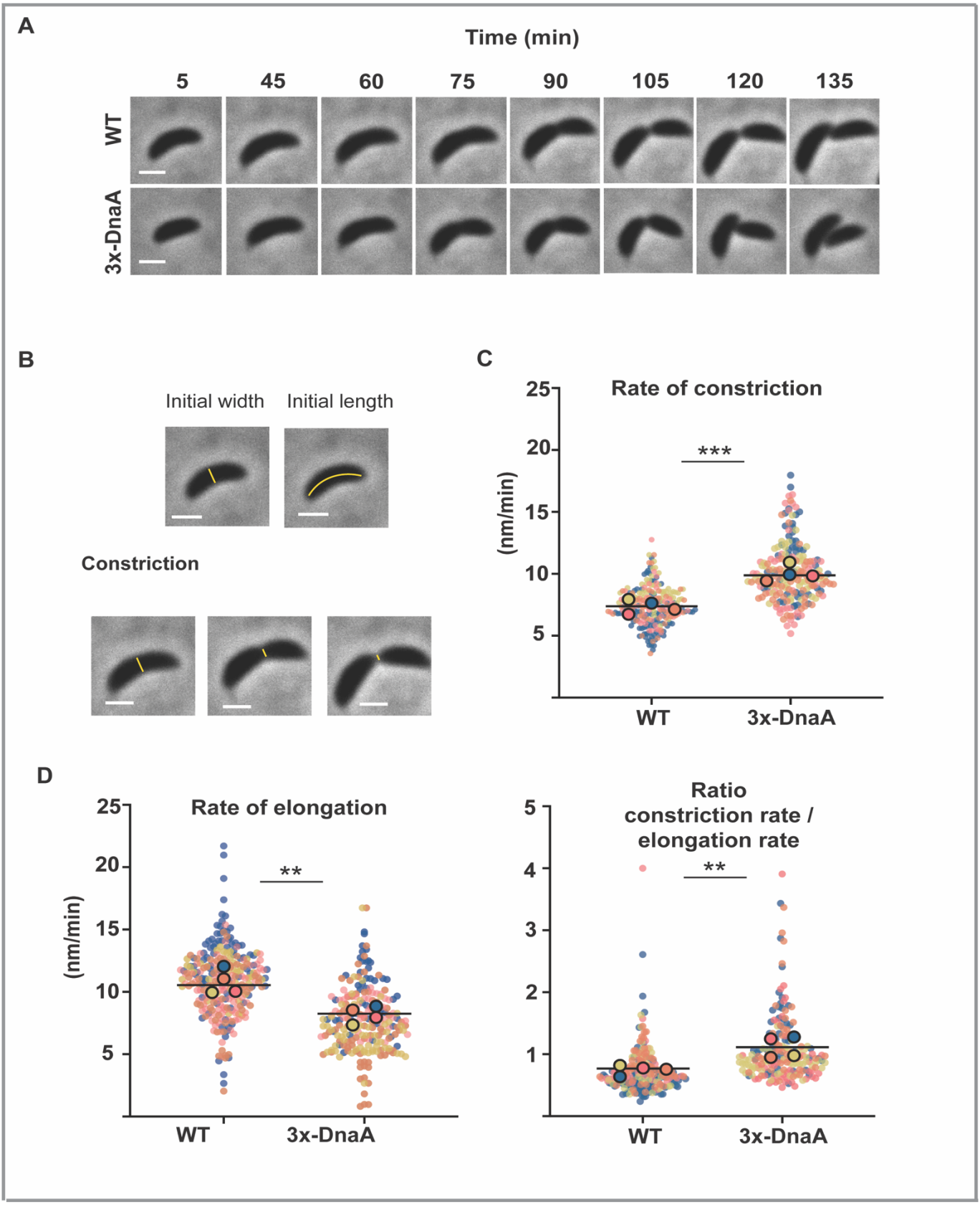
A
Time (min)
5
45
60
75
90
105
120
135
WT
3x-DnaA
B
Initial width
Initial length
Constriction
C
Rate of constriction
(nm/min)
25
20
15
10
5
***
WT
3x-DnaA
D
Rate of elongation
(nm/min)
25
20
15
10
5
**
WT
3x-DnaA
Ratio
constriction rate /
elongation rate
5
4
3
2
1
**
WT
3x-DnaA